Bulletin of the Seismological Society of America, Vol. 94, No. 4, pp. 1195–1206, August 2004

A Source Study of the Bhuj, India, Earthquake of 26 January 2001 (M_w 7.6)

by S. K. Singh, J. F. Pacheco, B. K. Bansal, X. Pérez-Campos, R. S. Dattatrayam, and G. Suresh

Abstract We study the source time function (STF) and radiated seismic energy (E_R) of the M_w 7.6 Bhuj earthquake using the empirical Green's function (EGF) technique. Our estimations of the STF and E_R are based on teleseismic *P* waves and regional seismograms, respectively. We find that the STFs as a function of azimuth have a similar shape and nearly constant duration of 18 sec. This suggests that the rupture propagation was essentially radial. The STFs show a sharp rise in the first 6 sec. The E_R estimated from the EGF technique is 2.1×10^{23} erg. We find that E_R's computed from integration of corrected velocity-squared spectra of teleseismic *P* waves and regional seismograms are in excellent agreement with the E_R obtained from the EGF technique. Since the seismic moment, M_0, is 3.4×10^{27} dyne cm, we obtain $E_R/M_0 = 6.2 \times 10^{-5}$. The radiation efficiency, η_R, during the Bhuj earthquake was low, about 0.23. The sharp rise of the STFs and $\eta_R = 0.23$ can be explained by Sato and Hirasawa's (1973) quasi-dynamic, circular source model with an effective stress of ~300 bar and the ratio of rupture to shear-wave velocity, V_R/β, of ~0.5. The corresponding estimate of slip velocity at the center of the fault is 156 cm/sec. $V_R/\beta \sim 0.5$ is in reasonable agreement with the duration of the STF and the reported dimension of the aftershocks, as well as with the results of inversion of teleseismic body waves.

The observations may also be explained by a frictional sliding model, with gradual frictional stress drop and significant dissipation of energy on the fault plane. This model requires an average dynamic stress drop of about 120 bar and $V_R/\beta \sim 0.7$ to explain both the rapid rise in the first 6 sec of the STFs and, along with a static stress drop of 200 bar, the observed E_R/M_0. High static stress drop is a common feature of most crustal earthquakes in stable continental regions. An examination of the available data, however, does not suggest that most of them also have relatively low radiation efficiency.

Introduction

The major, crustal Bhuj, India, earthquake of 26 January 2001 (M_w 7.6) caused devastation to the state of Gujrat, killing about 20,000 persons and injuring many more. It was India's most deadly earthquake in recorded history. The earthquake left nearly half a million people homeless and destroyed about 350,000 dwellings. Because of the catastrophe resulting from the earthquake and the fact that large crustal earthquakes in stable continental regions are infrequent, the source studies of the Bhuj earthquake have been focus of attention for many scientific groups in India and abroad.

Several groups have studied the aftershock distribution (e.g., Negishi *et al.*, 2002; Bodin and Horton, 2004). The aftershock area is rather compact and defines a rupture plane that strikes nearly east–west and dips to the south, suggesting that the nodal plane with strike $\phi = 66°$, dip $\delta = 64°$, and rake $\lambda = 60°$, reported in the Harvard Centroid Moment Tensor (CMT) catalog (Table 1, Fig. 1), is the fault plane. The aftershocks cover a depth range of 10–35 km and delineate an area of about 40 km × 33 km. The relatively small aftershock area and large seismic moment yields a relatively high static stress drop, $\Delta\sigma_s$, of about 200 bar.

Teleseismic body waves have been inverted to map the slip on the fault (Kikuchi and Yamanaka, 2001; Mori, 2001; Yagi and Kikuchi, 2001; Antolik and Dreger, 2003). The inversion of Yagi and Kikuchi (2001) suggests a slightly larger rupture area than the aftershock area and rupture propagation toward the west. Based on damage and intensity patterns, Bendick *et al.* (2001) and Hough *et al.* (2002) also inferred westward source directivity. The slip areas mapped by Kikuchi and Yamanaka (2001) and Mori (2001) are in better agreement with the aftershock area and indicate little, if any, directivity. Antolik and Dreger (2003) found that ~70% of the seismic release occurred in a small area (~375

Table 1
Source Parameters of the Bhuj Mainshock and the Aftershocks Used as EGFs

Date, Time	Latitude (°N)	Longitude (°E)	Depth (km)	M_0 (dyne cm)	M_w	Focal Mechanism		
						Strike (°)	Dip (°)	Rake (°)
26 January 2001, 03:16*	23.41	70.18	20	3.4×10^{27}	7.62	66	64	60
28 January 2001, 02:15†	23.61	70.46	15	7.4×10^{24}	5.85	79	51	72
8 February 2001, 16:54‡	23.63	70.45	25	8.0×10^{23}	5.20	75	55	100
19 March 2001, 08:24§	23.60	70.16	13	2.8×10^{24}	5.55	90	49	101

*Epicentral location from India Meteorological Department; depth, M_0, and focal mechanism from Harvard CMT catalog.

†Epicentral location from India Meteorological Department; depth and focal mechanism from Harvard CMT catalog; M_0 from this study. The M_0 listed in the Harvard CMT catalog is 5.2×10^{24} dyne cm.

‡Epicentral location from India Meteorological Department; depth from P. Mandal (personal comm., 2002); M_0 and focal mechanism from local and regional data (this study).

§Location and depth from P. Bodin (personal comm., 2002); M_0 from local and regional data (this study); and focal mechanism from Harvard CMT. The M_0 listed in the CMT is catalog 1.5×10^{24} dyne cm.

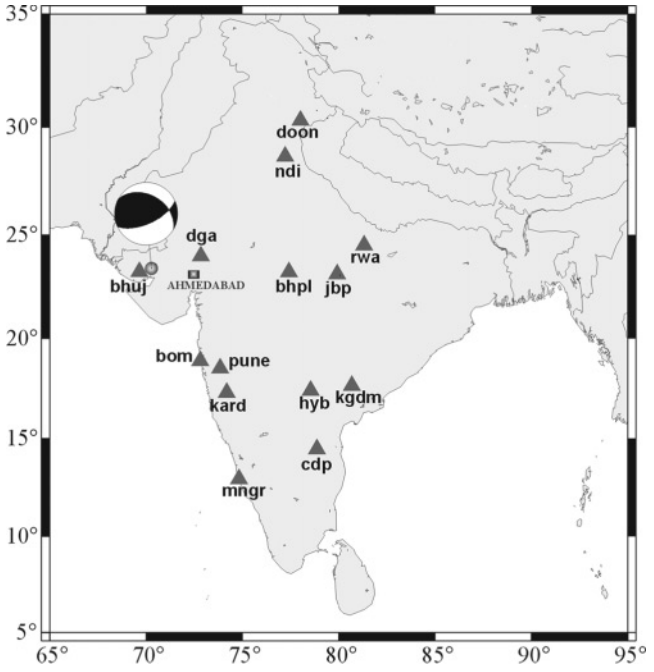

Figure 1. Map showing epicenter of the Bhuj earthquake (dot) and its focal mechanism. Regional seismological stations whose recordings were used in this study are indicated by triangles.

km^2) surrounding the hypocenter in the depth range of ~13–26 km. They also reported an indication of slip on a shallower area west of the hypocenter. However, the ground motions predicted by this source model only partially explain the observed intensities (figures 8 and 9 of Antolik and Dreger [2003]).

In this article, we analyze teleseismic- and regional-wave data (1) to study the azimuthal variation of source time functions (STFs) and (2) to determine the radiated seismic energy, E_R. We obtain STFs by deconvolving the mainshock records by those of the aftershock of 28 January 2001 (M_w 5.8). The radiated seismic energy is estimated using two methods: (1) deconvolution of the mainshock by some appropriate aftershocks recorded at regional distances and (2) integration of corrected velocity-squared spectra of teleseismic *P* waves and regional *S* waves. The STFs shed some light on the question of directivity and allow us to estimate the average dynamic stress drop (or, effective stress) acting on the fault. From the estimated radiated energy and average dynamic stress drop, in conjunction with the seismic moment and static stress drop, we infer some details of the rupture process of this important event.

Our results may be useful in understanding the seismotectonics of the Kutch region and in the estimation of seismic hazard in the area. The Bhuj earthquake has been suggested as an analog of the large New Madrid earthquakes of 1811 and 1812 (e.g., Ellis *et al.*, 2001). Thus, our study may also have useful implications for the New Madrid seismic zone.

STFs and Their Azimuthal Variation

We estimated STFs of the Bhuj earthquake and their variation with azimuth by deconvolving mainshock records by those of an aftershock recorded at the same site. The aftershock acts as an empirical Green's function (EGF) at frequencies that are smaller than its corner frequency. The method assumes that the location and focal mechanism of the mainshock and the EGF are similar. The main advantage of using an EGF comes from the fact that propagation, attenuation, and site effects are automatically included in the record. These effects are poorly known in most regions. Clearly, it is desirable to use as small an aftershock as possible. However, a practical limit is often imposed by the signal-to-noise ratio.

Teleseismic *P* Waves

At teleseismic distances only the largest aftershock of 28 January 2001 (M_w 5.8) gave rise to usable seismograms. The focal mechanism and the centroid location of these two

events are roughly similar (Table 1). Our analysis of teleseismic records is based on *P* waves. We used an iterative time-domain deconvolution technique developed by Ligorría and Ammon (1999). A Gaussian filter, $\exp(-\pi^2 f^2/a^2)$, was applied to velocity seismograms prior to deconvolution. Tests were carried out to determine the appropriate bandwidth parameter, a, of the filter. For both teleseismic and regional data, $a = 0.75$ Hz gave stable STFs. For $a = 0.75$ Hz, the filter amplitude is less than or equal to 0.1 at $f \geq 0.5$ Hz. Since, as discussed later, the corner frequency of the aftershock is 0.4 Hz, this is an acceptable EGF for the filtered seismograms.

Figure 2 shows the STFs as a function of station azimuth, ϕ_s. The top frame gives an example of the signal used in the analysis. We note that there is only one station in the azimuthal range of $80° < \phi_s < 280°$. The STFs at stations WRAB, KMI, LSA, SSE, and XAN have exceptionally small amplitudes and/or are more complex than those at other stations. This is probably because these stations are close to the node for the *P* wave of the mainshock. Ignoring these stations, the STFs have nearly the same total duration, τ, and have a similar shape. The average τ is ~18 sec. The STF catalog of the University of Michigan reports $\tau = 19$ sec. The STFs in Figure 2 are very similar to the point source STF determined by Antolik and Dreger (2003) from inversion of teleseimic body waves. The sharp rise time of the STFs, about 6 sec in duration, suggests a very large slip near the hypocenter at the beginning of the rupture (see also Mori [2001], Antolik and Dreger [2003]). We investigated whether the complexities seen in the falling part of the STFs could be explained by source directivity. We could not, however, track the timing of the complexities as a function of azimuth in a consistent fashion. We conclude that the source was essentially symmetric during the initial part of the rupture (which we will call the rupture of the main asperity), when a major part of the moment release occurred. The complexities seen in the STFs after about 9.5 sec correspond to the rupture of further subevents. These subevents may have occurred toward the west of the hypocenter at shallower depth as reported by Antolik and Dreger (2003). From finite-fault inversion of the teleseismic body waves, Antolik and Dreger (2003) found that ~70% of the moment release, $\sim 2.4 \times 10^{27}$ dyne cm, occurred during the rupture of the main asperity, whose dimension was about 25×15 km^2.

We model the rising part of the STF, which is similar at different stations, by the simple, quasi-dynamic, circular source model of Sato and Hirasawa (1973), henceforth called the "S&H model." In this model the rupture initiates at a point and spreads radially at a constant speed, V_R, until it stops. The slip on the fault at each instant follows the static solution of a circular crack under uniform shear stress, σ (Eshelby, 1957). We interpret σ as the effective stress (Brune, 1970). Figure 3 compares observed and synthetic STFs at KONO. In computing synthetics, we have taken $\alpha = 6.2$ km/sec, $\beta = 3.5$ km/sec, $\rho = 2.85$ g/cm^3, $\phi_s = 0°$, and $\theta = 35°$. Here θ is the angle between the normal to the fault and the takeoff angle. The pulse shape is independent of the azimuth, ϕ_s. The angle θ is $35° \pm 5°$ for all of the stations except two. The initial part of the radiated *P* pulse depends on σ and V_R/β but not on the seismic moment, M_0. In the computation of synthetics, however, we have taken $M_0 = 2.24 \times 10^{27}$ dyne cm (M_w 7.5), which is roughly equal to the seismic moment of the main asperity. The observed STF at KONO has been normalized such that the area under the pulse equals the seismic moment of the earthquake reported in the Harvard CMT catalog, that is, $M_0 = 3.4 \times 10^{27}$ dyne cm. The synthetic STF has been computed by normalizing the *P*-wave pulse such that the area equals the seismic moment of $M_0 = 2.24 \times 10^{27}$ dyne cm (M_w 7.5). From Figure 3 we note that the initial part of the observed STF at KONO is well fit with σ between 50 and 300 bar for V_R/β between 0.9 and 0.5. Antolik and Dreger (2003) found the best fit to the data using $V_R = 2.2$ km/sec ($V_R/\beta \sim 0.56$ in the lower crust and 0.69 in the upper crust). They reported, however, that V_R is poorly constrained. Assuming that the *P* pulse from the main asperity can be approximated by an isosceles triangle and noting that the rise time of the pulse is about 6 sec, we estimate the total duration of the pulse τ as 12 sec. Since the corresponding length, L, is 25 km, it follows that $V_R \sim L/\tau = 2.1$ km/sec and $V_R/\beta \sim 0.6$. A value of V_R/β between 0.5 and 0.75 and, hence, a value of σ between 100 and 300 bar for the Bhuj earthquake seems likely. We reiterate that this combination of σ and V_R/β only explains the initial part of the STF. In the S&H model, the slip velocity at the center of the fault, V_0, is given by

$$V_0 = (24/7\pi)(\sigma V_R/\mu) = 1.1(V_R/\beta)(\sigma\beta/\mu). \quad (1)$$

Assuming the rigidity $\mu = 3.7 \times 10^{11}$ dyne/cm^2, equation (1) gives a slip velocity between 83 and 156 cm/sec. This range of slip velocity on the fault roughly agrees with the estimated ground velocity of 40–55 cm/sec at hard sites in the epicentral region (Singh *et al.*, 2003).

Regional Love Waves

We also used regional recordings to study the azimuthal variation of STFs. The stations used in the analysis are shown in Figure 1. They are located at distances exceeding 550 km and cover an azimuthal range of 44°–149°. The seismograms were filtered with the same Gausian filter as the teleseismic records ($a = 0.75$ Hz). We found that the transverse component yielded the most stable STFs. The top frame of Figure 4 illustrates the signal used in the analysis. The results are shown in the bottom panel of Figure 4. As in the case of teleseismic *P* waves, the STFs have a similar shape and roughly the same duration, τ. However, the duration is only about 12 sec, much less than the 18 sec estimated from teleseismic *P* waves. This probably is a consequence of the aftershock of 28 January 2001 not being an adequate EGF for the later part of the mainshock rupture. We postulate that

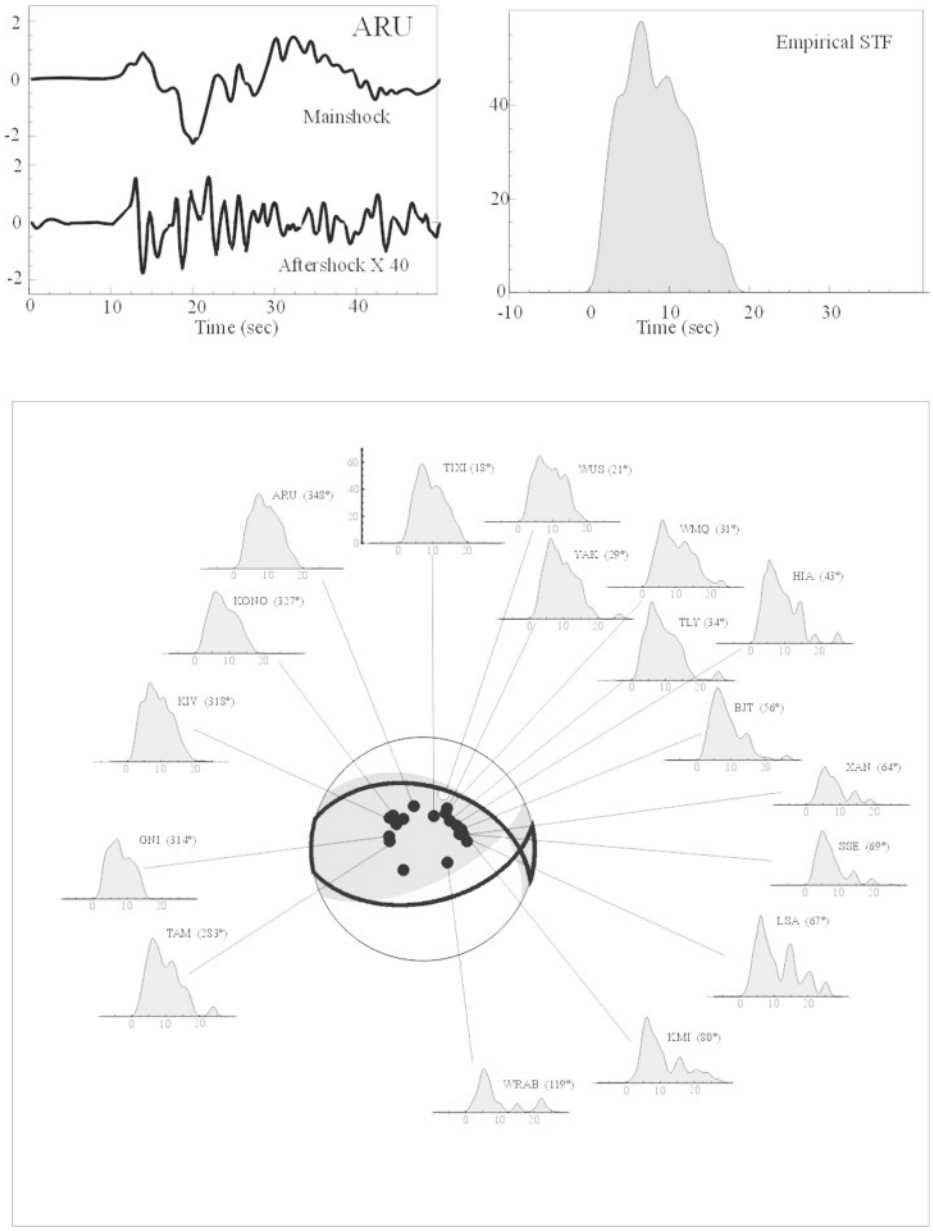

Figure 2. STFs retrieved from deconvolution of teleseismic *P* waves of the mainshock by those of the 28 January 2001 aftershock (M_w 5.8). Top left: *P* waves of the mainshock and the aftershock at ARU. Top right: STF at ARU.

the depth of the EGF was close to the centroid depth of the main asperity. Hence, the deconvolution returns the STF of this subevent, but not for the later part of the rupture, which took place at a different (presumably shallower) depth. This suggests that the aftershock was reasonable as an EGF for the teleseismic *P* waves for the entire rupture but was inadequate as an EGF for the later, shallower rupture when analyzing regional surface waves. This may be a consequence of long-period signals used in the analysis. At long periods, the EGF for teleseismic *P* waves is not very sensitive to depth. However, the depth of the source plays a critical role in the excitation of long-period, regional surface waves.

Estimation of Radiated Seismic Energy

An important source parameter of an earthquake is the radiated seismic energy, E_R. A reliable estimation of E_R, however, still remains problematic. The computed E_R of an earthquake by different authors often differs significantly, even when the data set used is the same. E_R estimates from teleseismic *P* waves and regional *S* waves can differ by an order of magnitude (Singh and Ordaz, 1994), reflecting the uncertainties in the corrections applied to the seismograms. It is not surprising, therefore, that accurate estimation of E_R is presently an active field of research (e.g., Prejean and

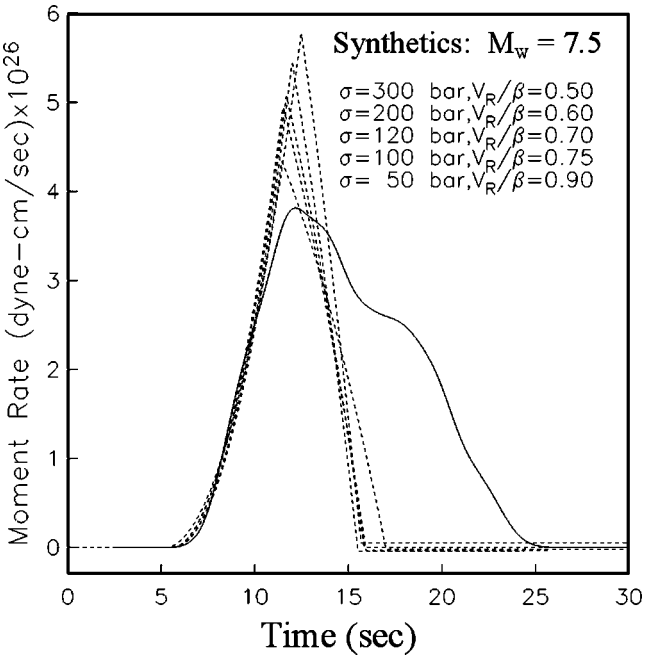

Figure 3. STF at KONO (continuous line). The area under the curve equals the seismic moment of the earthquake ($M_0 = 3.4 \times 10^{27}$ dyne cm). Synthetic STFs (dashed lines) were generated using Sato and Hirasawa's (1973) circular model for various combinations of stress and rupture to shear-wave velocity (V/β) (see text).

Ellsworth, 2001; Boatwright *et al.*, 2002; Venkataraman, 2002; Ide *et al.*, 2003; Pérez-Campos *et al.*, 2003). In this section, we estimate the E_R of the Bhuj earthquake using regional and teleseismic waves.

One powerful technique to obtain a reliable estimate of E_R is through deconvolution of the mainshock by appropriate aftershocks. The aftershocks act as EGFs. It is based on the assumptions that the mainshock and aftershock locations and focal mechanisms are similar. This method was applied by Venkataraman *et al.* (2002) to the regional recordings of the Hector Mine, California, earthquake of 16 October 1999 ($M_w = 7.1$). The estimated E_R values were tightly clustered over distance and over different aftershocks used as EGFs. The precise and accurate estimate of E_R was then used to calibrate teleseismic estimates. We use the EGF technique on regional seismograms to estimate the E_R of the mainshock. We also compute E_R directly from the regional seismograms and from teleseismic *P* waves. We compare different estimates of E_R with the E_R obtained from the EGF method to investigate whether the calibrations made for other regions are also valid for the Indian shield region.

E_R from Regional Data using Aftershocks as EGFs

The moment rate spectrum, $\dot{M}_0(f)$, of the mainshock can be obtained from the spectral ratio of the mainshock and the aftershock recordings and multiplying the ratio by the seismic moment of the aftershock. The radiated seismic energy, E_R, is computed from $\dot{M}_0(f)$ using the relation (Vassiliou and Kanamori, 1982)

$$E_R = (4\pi/5\ \rho\beta^5) \int_0^\infty f^2 \dot{M}_0^2\ (f) df, \qquad (2)$$

where $\dot{M}_0(f)$ is the moment rate spectrum, ρ is the density, and β is the shear-wave velocity. Equation (2) neglects seismic energy in *P* waves since it contributes only 5% of the total E_R. For a reliable estimation of E_R, the corner frequency, f_c, of the mainshock should be much smaller than the corner frequency of the aftershock so that the source spectrum, obtained by spectral division, is valid for as large f/f_c as possible. Useful regional broadband recordings of the Bhuj mainshock are available at distances exceeding 550 km. At these distances only larger aftershocks have useful signal-to-noise ratios. Table 1 lists the three aftershocks whose recordings were selected as EGFs to determine the moment rate spectrum.

We first examined the moment rate spectra, $\dot{M}_0(f)$, of the mainshock and the aftershocks computed directly from the spectra of the *S*-wave group recorded at regional distances (550 km $< R <$ 1600 km). The spectra were corrected for geometrical spreading (R^{-1} out to $R = 100$ km and $R^{-0.5}$ at larger distances) and anelastic attenuation ($Q = 508f^{0.48}$). We took $\rho = 2.85$ g/cm^3 and $\beta = 3.5$ km/sec (see Singh *et al.* [1999] for other parameters and the details of the method). Figure 5 shows the moment rate spectra and theoretical ω^{-2}-source spectra that, visually, fit them. We note that the $\dot{M}_0(f)$ of the mainshock is remarkably well explained by the ω^{-2} source spectrum with $M_0 = 3.4 \times 10^{27}$ dyne cm (a fact also noted by J. Boatwright [personal comm., 2002]) and $f_c = 0.05$ Hz. Aftershock studies suggest that the total rupture area of the Bhuj earthquake was about 40 $\times$ 33 km^2 (Horton *et al.*, 2001; Negishi *et al.*, 2002). This gives an equivalent source radius, *a*, of about 21 km. Brune's (1970) model relates *S*-wave corner frequency, f_c, to source radius *a* by $f_c = 0.372\beta/a$. This yields $f_c = 0.06$ Hz, a value close to $f_c = 0.05$ Hz, which fits the moment rate spectrum. The moment rate spectrum of the 28 January 2001 aftershock (Fig. 5, top right panel) deviates from the ω^{-2} model between 0.15 and 1.5 Hz; the observed spectral falloff in this band is close to ω^{-1}. An ω^{-2} source model required to fit the low- and high-frequency level gives $M_0 = 7.4 \times 10^{24}$ dyne cm and $f_c = 0.37$ Hz. We note that the M_0 listed in the CMT catalog is 5.2×10^{24} dyne cm. The moment rate spectra of the aftershocks of 8 and 19 February 2001 are reasonably well explained by the ω^{-2} model. The estimated M_0 and f_c for these two events are 8.0×10^{23} dyne cm and 0.5 Hz and 2.8×10^{24} dyne cm and $f_c = 0.32$ Hz, respectively (Fig. 5, bottom panels). The seismic moment listed in the CMT catalog for the 19 February 2001 aftershock is 1.5 $\times 10^{24}$ dyne cm.

To estimate the E_R of the mainshock, we computed the mainshock/aftershock spectral ratio of each of the three com-

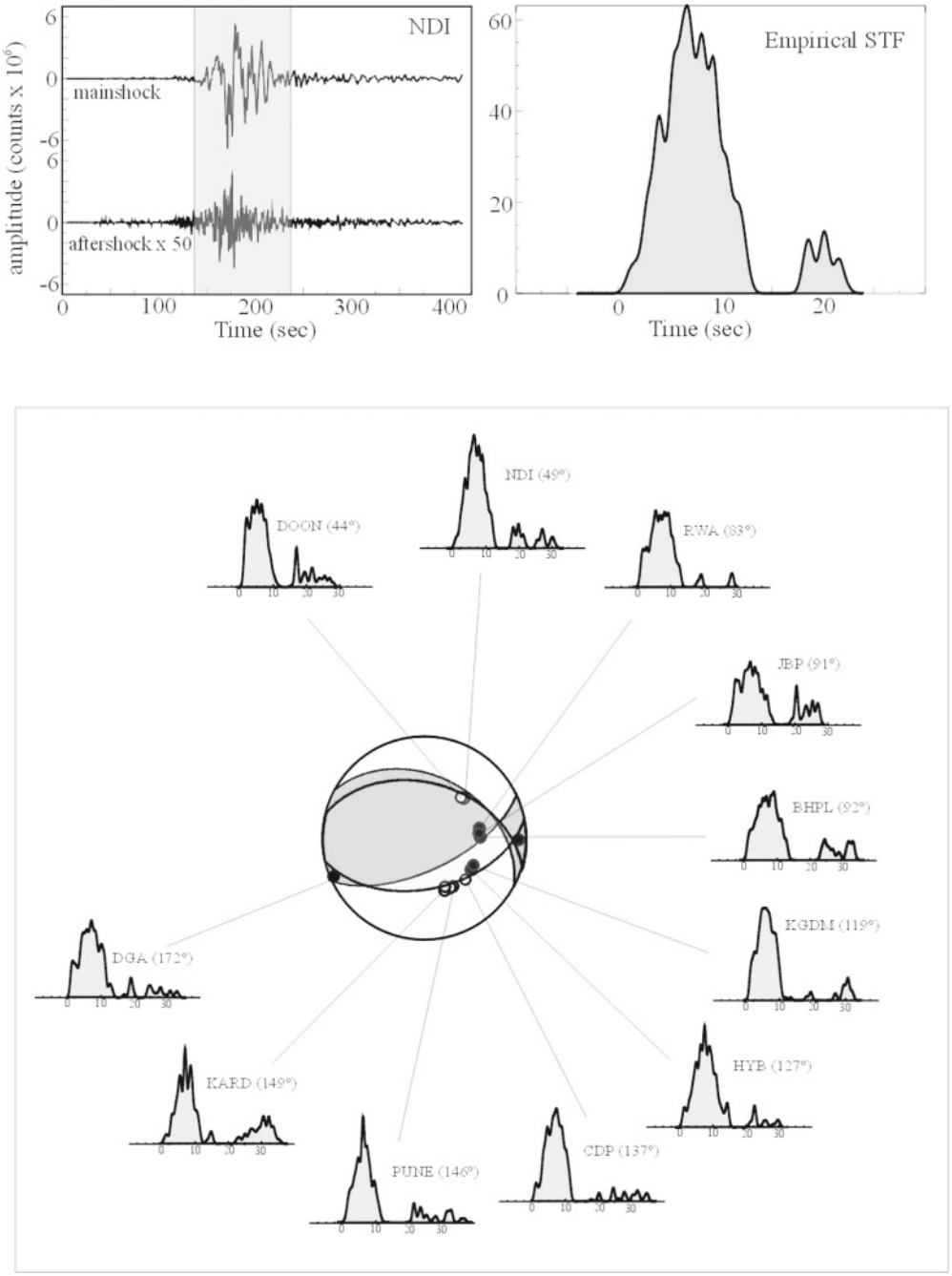

Figure 4. STFs retrieved from deconvolution of regional waves of the mainshock by those of the 28 January 2001 aftershock (M_w 5.8). Top left: Transverse component of the mainshock and the aftershock at NDI. Top right: STF at HYB.

ponents at each station. The signal used in computing the Fourier transform began at the arrival of the *S* wave, and the window length was roughly 120 sec. The Fourier transform was smoothed with a 1/3 octave band filter before computing the spectral ratio, which then was multiplied by the seismic moment of the aftershock to obtain the moment rate spectrum, $\dot{M}_0(f)$, of the mainshock. Figure 6 shows the $\dot{M}_0(f)$ corresponding to each of the aftershocks. Superimposed on these figures is the theoretical $\dot{M}_0(f)$ for an ω^{-2} source model, with $M_0 = 3.4 \times 10^{27}$ dyne cm and an *S*-wave corner frequency, f_c, of 0.05 Hz. From these figures we obtain the frequency range, f_1–f_2, which can be used in the estimation of E_R. We note that $f_1 = 0.030$ Hz and $f_2 = 0.160$ Hz, except for the 19 February event, for which $f_2 = 0.145$ Hz. Below f_1, the spectra are not reliable because of the low signal-to-noise ratio of the EGFs (the aftershocks). Above f_2, the spectra significantly deviate from the ω^{-2} source model because the corner frequencies of the EGFs are

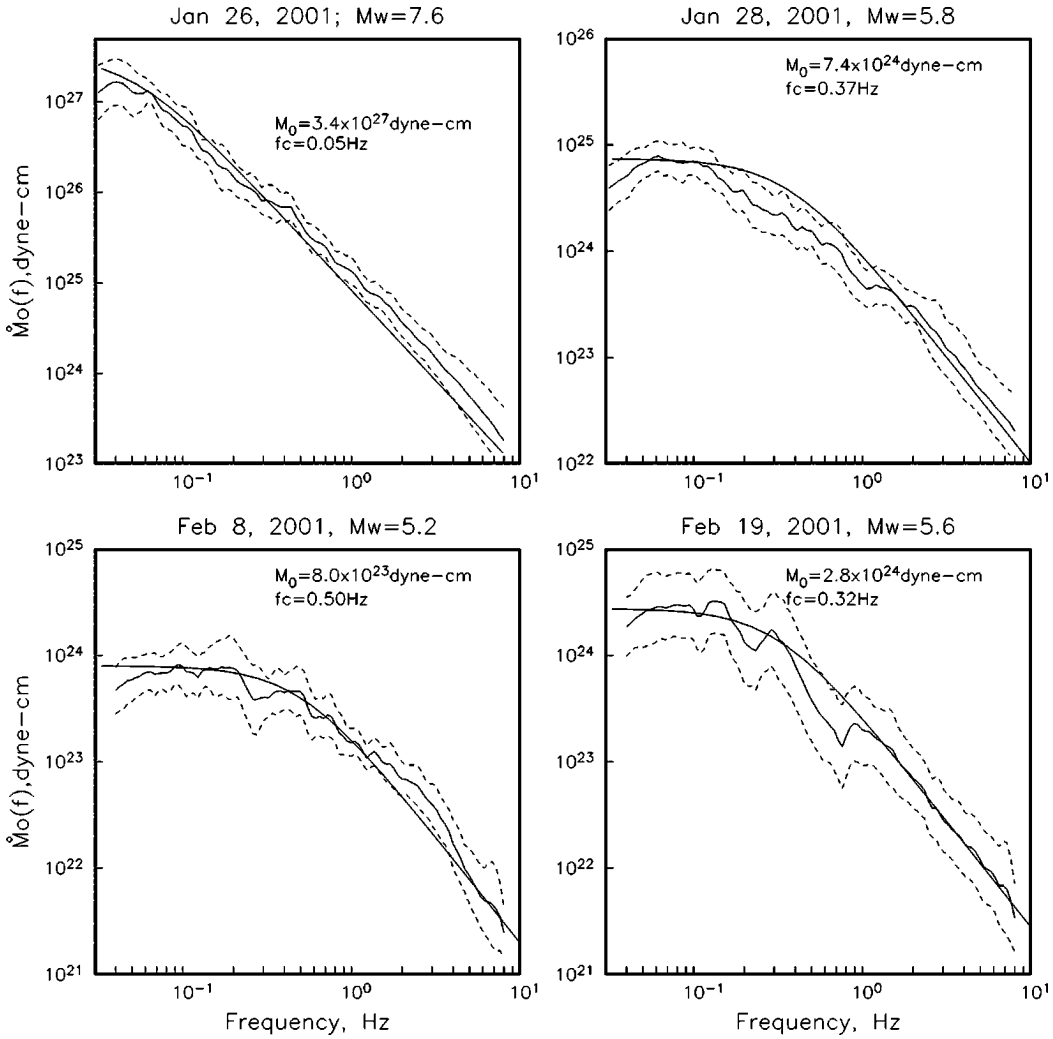

Figure 5. Moment rate spectra (median ± 1 s.d. curves) of the mainshock and three aftershocks obtained from regional *S* recordings. Continuous curves correspond to the ω^{-2} source model.

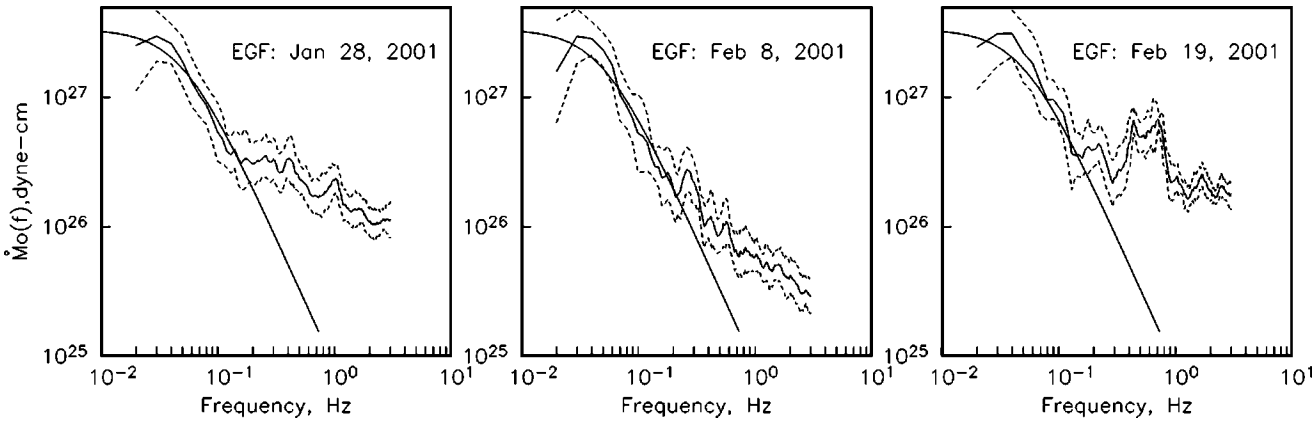

Figure 6. Moment rate spectrum of the mainshock (median ± 1 s.d. curves), estimated from spectral ratio of mainshock to the aftershocks. Superimposed is the curve for an ω^{-2} source model.

not sufficiently separated from that of the mainshock. We accounted for the missing energy between 0 and 0.03 Hz by assuming an ω^{-2} source in equation (2), with $M_0 = 3.4 \times 10^{27}$ dyne cm and $f_c = 0.05$ Hz. This gives $E_R = 1.1 \times 10^{22}$ erg. The total seismic energy was obtained by summing 1.1×10^{22} erg to the energy contained in the frequency range of f_1 and f_2 and then computing the percentage of E_R included in the frequency band of 0–f_2 Hz for an ω^{-2} source (see Singh and Ordaz, 1994). For example, with the 28 January aftershock as the EGF, the median E_R in the frequency range of 0–0.16 Hz is 1.14×10^{23} erg. We note that in this case $f_2/f_c = 3.2$. For an ω^{-2} source, E_R between 0 and $f_2/f_c = 3.2$ includes about 63% of the total E_R. Hence the total E_R during the Bhuj earthquake is estimated as (1.14/0.63) $\times 10^{23}$ erg $= 1.8 \times 10^{23}$ erg. Table 2 lists the E_R estimated using each of the aftershocks as the EGF. For the entire data set, log $E_R = 23.324 \pm 0.195$, which gives a median of $E_R = 2.11 \times 10^{23}$ erg. If the corner frequency of the mainshock is taken as 0.06 Hz, then the estimated E_R will be about 10% higher.

We emphasize that roughly 40% of the total E_R has been estimated assuming an ω^{-2} source spectrum. In as much as the Bhuj mainshock closely follows this model, we expect no gross error in our estimation due to this assumption. For an ω^{-2} source, equation (2) reduces to $E_R = 7.89 M_0^2 f_c^3/\mu\beta^3$. With $M_0 = 3.4 \times 10^{27}$ dyne cm, $f_c = 0.05$ Hz, and $\mu = 3.7 \times 10^{11}$ dyne/cm^2, we obtain $E_R = 1.94 \times 10^{23}$ erg, which is almost the same as the median E_R of 2.11×10^{23} erg.

A significant error in our estimation of E_R, listed in Table 2, may occur if the seismic moment of the aftershock used as the EGF is in error. For example, the M_0's reported in the Harvard CMT catalog for the aftershocks of 28 January and 19 February are smaller than those estimated in this study by factors of 1.42 and 1.80, respectively. If the CMT moments are the correct ones, then the E_R in Table 2, obtained with 28 January and 19 February events as EGFs, should be decreased by factors of 2.02 and 3.24, respectively. Note that the amplitudes of the moment rate spectra of the mainshock obtained using the three aftershocks as empirical EGFs are equal around $f = 0.03$ Hz (Fig. 5). This gives us confidence that the seismic moments of the aftershocks estimated from regional data (Fig. 4) are accurate and, thus, the E_R estimated earlier is not affected by the errors in the seismic moments of the EGFs.

Table 2
Radiated Seismic Energy during the Bhuj Mainshock (M_w 7.6) Estimated using Aftershocks as EGFs

EGF Used in the Estimation of E_R	No. Stations	log E_R (erg) $f_c = 0.05$ Hz
28 January 2001	9	23.299 ± 0.157
8 February 2001	5	23.258 ± 0.221
19 February 2001, 08:24	4	23.483 ± 0.182

E_R from Regional Data by Integrating Squared Velocity Spectra

Following Singh and Ordaz (1994), E_R can be written as

$$E_R = [4\pi R^2 \{G^2(R)/R^2\}\rho\beta/F^2] \cdot [2\int_0^\infty \{V_N^2(f) + V_E^2(f) + V_Z^2(f)\} e^{2\pi f R/\beta Q(f)} df, \quad (3)$$

where $V_j(f)$ is the velocity spectrum jth component of the S-wave group, R is hypocentral distance, and $G(R)$ is the geometrical spreading correction, which, as before, may be taken as $G(R) = R$ for $R \le R_x$ and $G(R) = (RR_x)^{1/2}$ for $R > R_x$. We chose $R_x = 100$ km. In equation (3), β is shear-wave velocity (3.5 km/sec), ρ is density (2.85 g/cm^3), F is the free-surface amplification (2.0), and $Q(f)$ is the quality factor. In this study, we take $Q(f) = 508 f^{0.48}$ reported by Singh *et al.* (1999) for the Indian shield region. The median E_R is 2.54×10^{23} erg.

We also estimated E_R from the regional data by correcting the spectra for site effects. The regional broadband stations, which recorded the earthquake, are situated on hard sites. For this reason, we applied the site effect correction for a generic rock site (Boore and Joyner, 1997). Figure 7 shows E_R as function of distance. The median E_R is now 1.67×10^{23} erg.

Estimated Radiated Seismic Energy from Teleseismic Waves

For the estimation of E_R using teleseismic data, we followed Boatwright and Choy (1986). The estimate of the energy flux was obtained from the integral of the squared velocity spectrum of the P-wave group (P, pP, and sP waves),

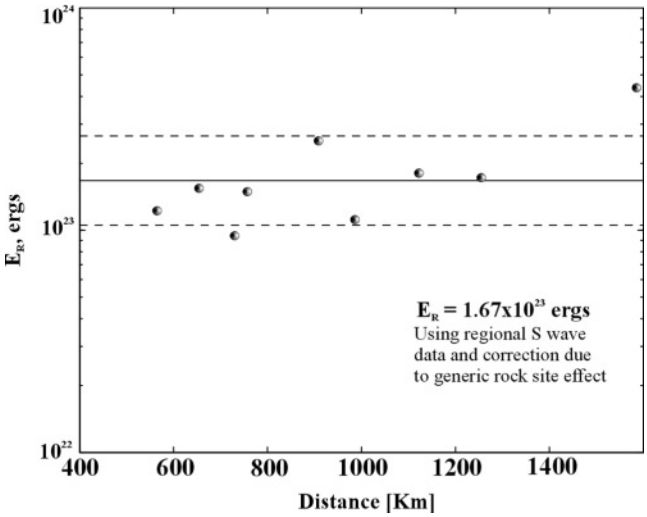

Figure 7. Radiated seismic energy estimated from regional data (corrected for generic rock site effect) plotted as function of distance.

corrected for attenuation and site effects. For the site effect correction, we used either a hard-rock generic amplification (Boore and Joyner, 1997) in combination with a local attenuation parameter $\kappa = 0.01$ sec (Pérez-Campos *et al.*, 2003) or a site correction modeled by Pérez-Campos (2002) if available. The total *P*-wave energy was then estimated using covariance-weighting least squares (Pérez-Campos and Beroza, 2001) and correcting for geometrical spreading and radiation pattern. Finally, we used $q = 15.58$ (Boatwright and Choy, 1986), the partitioning between *S*- and *P*-wave energy, to estimate the total radiated seismic energy as $E_R = 1.20 \times 10^{23}$ erg (Fig. 8).

Table 3 lists different estimates of E_R, including that by Venkataraman (2002), based on teleseismic *P* waves. In spite of the differences in the data sets, techniques used, and corrections applied, the estimates are surprisingly consistent: they all fall between 1.7 and 2.5×10^{23} erg. In the following, we shall take $E_R = 2.11 \times 10^{23}$ erg, obtained from the EGF method, as the radiated seismic energy from the Bhuj earthquake.

Static Stress Drop

There is consensus that the average static stress drop, $\Delta\sigma_s$, of the Bhuj earthquake was unusually high. However, the estimates of $\Delta\sigma_s$ vary among different authors. Negishi *et al.* (2002) and Bodin and Horton (2004) have used locations of the aftershocks, based on portable local networks of seismographs, to estimate $\Delta\sigma_s$. Negishi *et al.* (2002) found an equivalent source radius of 20–25 km and $\Delta\sigma_s$ between 126 and 246 bar, while Bodin and Horton (2004) estimated a rupture area of 1300 km^2 and $\Delta\sigma_s$ of 160 ± 20 bar. Antolik and Dreger (2003) used the area defined by 0.5-m slip contours and report a $\Delta\sigma_s$ of 210 bar. In the following we will assume $\Delta\sigma_s = 200$ bar.

Discussion and Conclusions

The similarity of the STFs of the Bhuj earthquake, shown in Figure 3, as function of azimuth, with nearly a constant pulse duration, τ, of about 18 sec, suggests that the rupture was essentially radial with little, if any, directivity toward the west. The initial 6 sec of the pulse can be explained by the S&H model. If V_R/β is restricted between 0.5 and 0.75, then the model predicts an effective stress, σ, between 100 and 300 bar accelerating the fault and a slip velocity of 83–156 cm/sec at the center of the fault. There is some support for a relatively small value of V_R/β. We recall that the aftershocks define a rectangular area of length $L = 40$ km and width $W = 33$ km or, equivalently, a circular area of radius $a = 21$ km. Thus, $V_R \sim (L/\tau) = 2.2$ km/sec, and hence $V_R/\beta \sim 0.64$. The results of the inversion of teleseismic body waves also suggest $V_R \sim 2.2$ km/sec, although the rupture velocity is not well constrained (Antolik and Dreger, 2003).

The radiated seismic energy, E_R, estimated using different methods was $\sim 2.1 \times 10^{23}$ erg. The source parameters E_R, M_0, and $\Delta\sigma_s$ are often interpreted in terms of apparent stress, σ_a, which is defined as $\sigma_a = \mu E_R/M_0$ (Aki, 1966; Wyss, 1970). For the Bhuj earthquake we obtain $\sigma_a = 23$ bar. Since $\sigma_a < \Delta\sigma_s/2$, the earthquake represents an overshoot model, that is, the final stress is smaller than the frictional stress (Savage and Wood, 1971).

The radiation efficiency, η_R, for the Bhuj earthquake was 0.23, where $\eta_R = E_R/(E_R + E_G) \sim 2(E_R/M_0)/(\Delta\sigma_s/\mu)$, and E_G is the fracture energy (Husseini, 1977; Venkataraman, 2002). Venkataraman (2002) has obtained reliable estimates of E_R and $\Delta\sigma_s$ for 23 large subduction zone earthquakes and six crustal earthquakes (including the Bhuj earthquake). The radiation efficiency of the Bhuj earthquake is among the lowest (only the deep 1994 Bolivian and 1999 Russia–China border earthquakes and the inslab 1993 Kushiro-oki earthquake have lower η_R's).

The observations on the source parameters of the Bhuj earthquake may grossly be explained by the S&H model. The radiation efficiency, η_R, defined earlier, is the same as η_v in equation (25) of Sato and Hirasawa (1973). From their table 3, $\eta_R = 0.23$ corresponds to $V_R/\beta \sim 0.5$. From our Figure 3, the effective stress, corresponding to $V_R/\beta \sim 0.50$, is about 300 bar. Ide (2002) has shown that the ratio of the static stress to effective stress in the S&H model is slightly less than 1. The ratio is 0.93 for $V_R/\beta \sim 0.50$, somewhat higher than 0.67 for the Bhuj earthquake.

An alternative explanation of the observations results

Table 3
Comparison of Estimated Radiated Seismic Energy, E_R

Data and Method	E_R (erg)	Reference
Regional data, EGF method	2.1×10^{23}	This study
Regional data, integrating squared-velocity spectra		
Without site effect correction	2.5×10^{23}	This study
After generic site effect correction	1.7×10^{23}	This study
Teleseismic *P*-wave data		
Integration of squared-velocity spectra	2.0×10^{23}	Venkataraman, 2002
Integration of squared-velocity spectra with site effect correction	1.2×10^{23}	This study
Theoretical ω^{-2} source model with *S*-wave corner frequency of 0.05 Hz	1.90×10^{23}	This study

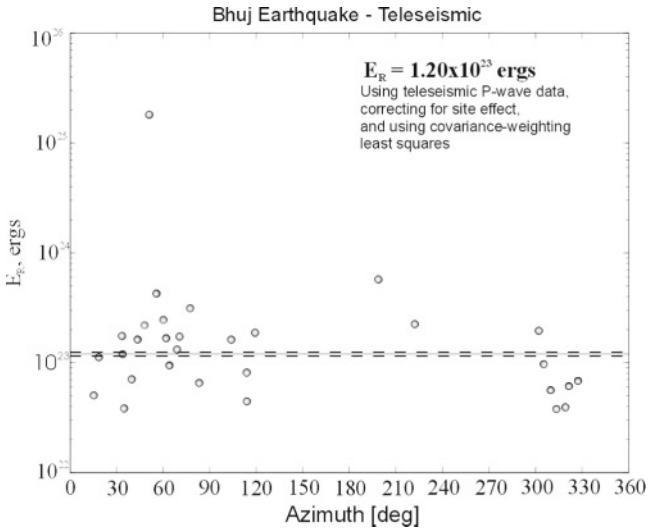

Figure 8. Radiated seismic energy estimated from teleseismic *P* waves (corrected for site effect) plotted as function of azimuth.

from the formulation of Kanamori and Heaton (2000), who expressed E_R/M_0 as

$$E_R/M_0 = (2\langle\Delta\sigma_d\rangle - \Delta\sigma_s)/2\mu, \quad (4)$$

where $\langle\Delta\sigma_d\rangle = \sigma_0 - \langle\sigma_f\rangle$ is the average dynamic stress drop, σ_0 is the initial stress, and $\langle\sigma_f\rangle$ is the dynamic friction during the rupture averaged over the slip. The static stress is, of course, given by $\Delta\sigma_s = \sigma_0 - \sigma_1$, where σ_1 is the final stress. As discussed by Kanamori and Heaton (2000), if friction drops rapidly then $\langle\Delta\sigma_d\rangle$ is comparable or larger than $\Delta\sigma_s$ and $E_R/M_0 \sim \Delta\sigma_s/2\mu$ so that $\eta_R = 1$. However, if the friction drops slowly, then $\langle\Delta\sigma_d\rangle$ roughly equals $(\sigma_0 + \sigma_1)/2$, the average stress, and the radiated energy is zero. Scaled energy, E_R/M_0, for the Bhuj earthquake is 6.2×10^{-5}. A rapid drop in friction, with $\Delta\sigma_s = 200$ bar, would have resulted in $E_R/M_0 \sim 2.7 \times 10^{-4}$, about 5 times greater than the observed value. Thus, the observations can be explained by a gradual drop in friction and a significant dissipation of energy on the fault plane. For the static stress drop of 200 bar, the observed E_R/M_0 requires an average dynamic stress drop of ~120 bar. If the average dynamic stress drop roughly equals the effective stress and V_R/β is about 0.7, then this also explains the rapid rise in the first 6 sec of the STF (Fig. 3).

Radiation efficiency, η_R, has obvious implications for the expected ground motions in the epicentral region. η_R becomes 1 as $V_R/\beta \rightarrow 1$ in the S&H model or if the frictional stress drop occurs rapidly (equation 4). In either case, this would result in higher slip velocity on the fault plane and larger peak ground velocities in the epicentral region.

A relatively high static stress drop for crustal earthquakes in stable continental regions is expected (Kanamori and Anderson, 1975). Is low radiation efficiency also common to such events? To answer this, we compiled relevant data of crustal, intraplate earthquakes. The data set consists of 16 earthquakes that were analyzed by Boatwright and Choy (1992) using spectral analysis of teleseismic *P* waves. It includes the Jabalpur earthquake of 1997 (M_w 5.8), an event located in the Indian shield whose radiated energy and stress drop were estimated from regional *S*-wave spectra by Singh *et al.* (1999). We compliment these data with those from five crustal earthquakes, located on diffused plate boundaries (Hector Mine, 1999, M_w 7.1; Chi-Chi, 1999, M_w 7.6; Izmit, 1999, M_w 7.6; Northridge, 1994, M_w 6.6; Landers, 1992, M_w 7.3) and analyzed by Venkataraman (2002). We also include the recent earthquake of central Kunlun (14 November 2001, M_w 7.9). For this strike-slip earthquake, the reported source parameters are $M_0 = 5.9 \times 10^{27}$ dyne cm (Harvard CMT catalog), $E_R = 3.2 \times 10^{23}$ erg (National Earthquake Information Center Catalog), a supershear rupture (Bouchon and Vallée, 2003), and rupture length, *L*, between 200 and 400 km (Lin et al., 2002). We assume the width $W = 20$ km and, using the relation $\Delta\sigma_s = 2M_0/(\pi LW^2)$, obtain a static stress drop between 23 and 47 bar and, hence, radiation efficiency between 0.68 and 1.36. Figure 9 (top) shows E_R/M_0 as a function of M_0. Generally, E_R/M_0 values are smaller for earthquakes analyzed by Boatwright and Choy (1992) than for the two events in the Indian shield and the six others that were located on diffused plate boundaries. This difference may be real, or it may an artifact of some systematic bias in the estimation of E_R. The plot of radiation efficiency, η_R, as function of moment (Fig. 9, bottom) shows that η_R is greater than 0.4 for one-third of the events. Indeed, η_R is greater than 1 for three of the events (Landers, Northridge, and central Kunlun). Again, some of the dispersion in the data must be due to errors in the estimation of the radiated energy and static stress drop. In any case, the available data do not suggest that η_R for intraplate, shallow earthquakes is systematically low.

Kanamori and Allen (1986) have studied the relationship between repeat times and the average stress drop of crustal earthquakes (including interplate and intraplate events but excluding subduction earthquakes). They reported that for crustal earthquakes of the same magnitude, those with shorter length have longer repeat times. This is because such events have higher stress drops, reflecting the greater strength of the causative fault. The length and magnitude of the Bhuj earthquake correspond to a repeat time of greater than 2000 yr. There is some support for this estimate of the repeat time. From paleoseismological evidence, which is constrained by historic data, the last earthquake in the adjacent Allah Bund area before the 1819 event ($M \geq 7.5$) occurred in A.D. 893 (Rajendran and Rajendran, 2001). For Bhuj, there are no data on past earthquakes. However, a preliminary assessment, mostly based on historical and archeological data, suggests that the recurrence interval could be much longer than 1000 yr (K. Rajendran, personal comm., 2002).

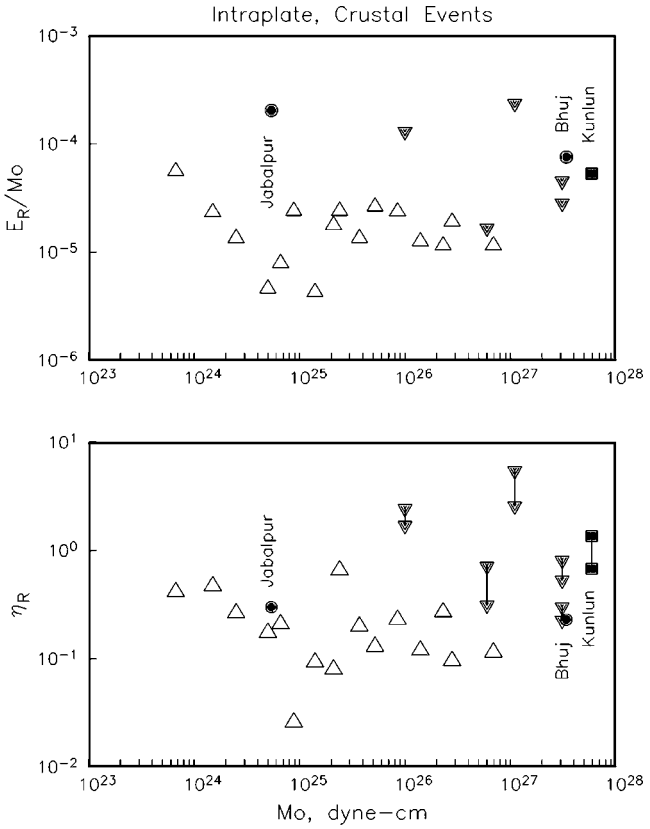

Figure 9. Scaled radiated energy, E_R/M_0, and radiation efficiency, η_R as a function of seismic moment, M_0, for intraplate, crustal earthquakes. Open triangles: data from Boatwright and Choy (1992). Inverted solid triangles: data from Venkataraman (2002).

Acknowledgments

We express our gratitude to the authorities of the following institutions in India for making data available: India Meteorological Department/ Department of Science and Technology; DEQ, I.I.T., Roorkee; National Geophysical Research Institute; Geological Survey of India; Gujrat Engineering Research Institute; Osmania University; Indian Institute of Geomagnetism, Mumbai; Wadia Institute of Himalyan Geology; Centre for Earth Science Studies; and National Institute of Rock Mechanics. We are grateful to the Director General of India Meteorological Department for permission to use the data. We thank the Secretary, DST, for his continuous support. A preliminary version of the manuscript was revised by Jack Boatwright. We thank Hiroo Kanamori, Tamao Sato, and the associate editor for their incisive comments. The research was partially supported by UNAM, DGAPA Projects IN111601.

References

Aki, K. (1966). Generation and propagation of G waves from the Niigata earthquake of June 16, 1964. Part 2. Estimation of earthquake moment from G wave spectrum, *Bull. Earthquake Res. Inst. Tokyo Univ.* **44,** 73–88.

Antolik, M., and D. S. Dreger (2003). Rupture process of the 26 January 2001 M_w 7.6 Bhuj, India, earthquake from teleseismic broadband data, *Bull. Seism. Soc. Am.* **93,** 1235–1248.

Bendick, R., R. Bilham, E. Fielding, V. K. Gaur, S. E. Hough, G. Kier, M. N. Kulkarni, S. Martin, K. Mueller, and M. Mukul (2001). The 26 January 2001 "Republic Day" earthquake of India, *Seism. Res. Lett.* **72,** 328–335.

Boatwright, J., and G. L. Choy (1986). Teleseismic estimates of the energy radiated by shallow earthquakes, *J. Geophys. Res.* **91,** 2095–2112.

Boatwright, J., and G. L. Choy (1992). Acceleration source spectra anticipated for large earthquakes in northeastern North America, *Bull. Seism. Soc. Am.*, **82,** 660–682.

Boatwright, J., G. L. Choy, and L. C. Seekins (2002). Regional estimates of radiated energy, *Bull. Seism. Soc. Am.* **92,** 1241–1255.

Bodin, P., and S. Horton (2004). Source parameters and tectonic implications of aftershocks of the M_w 7.6 Bhuj earthquake of January 26, 2001, *Bull. Seism. Soc. Am.* **94,** 818–827.

Boore, D. M., and W. B. Joyner (1997). Site amplifications for generic rock sites, *Bull. Seism. Soc. Am.* **87,** 327–341.

Bouchon, M., and M. Vallée (2003). Observation of long supershear rupture during the magnitude 8.1 Kunlunshan earthquake, *Science* **301,** 824–826.

Brune, J. N. (1970). Tectonic stress and the spectra of seismic shear waves from earthquakes, *J. Geophys. Res.* **75,** 4997–5009.

Centroid Moment Tensor (CMT) Catalog, www.seismology.harvard.edu/CMTsearch.html (last accessed September 2003).

Ellis, M., J. Gomberg, and E. Schweig (2001). Indian earthquake may serve as analog for the New Madrid earthquakes, *EOS* **82,** 345–350.

Eshelby, J. D. (1957). The determination of the elastic field of an ellipsoidal inclusion and related problems, *Proc. R. Soc. London* **241,** 376–396.

Hough, S. E., S. Martin, R. Bilham, and G. M. Atkinson (2002). The January 26, 2001 *M* 7.6 Bhuj, India earthquake: observed and predicted ground motions, *Bull. Seism. Soc. Am.* **92,** 2061–2079.

Husseini, M. I. (1977). Energy balance for formation along a fault, *Geophys. J. R. Astr. Soc.* **49,** 699–714.

Ide, S. (2002). Estimation of radiated energy of finite-source earthquake models, *Bull. Seism. Soc. Am.* **92,** 2994–3005.

Ide, S., G. C. Beroza, S. G. Prejean, and W. L. Ellsworth (2003). Apparent break in earthquake scaling due to path and site effects on deep borehole recordings, *J. Geophys. Res.* **108,** no. B5, 2271, doi 10.1029/2001JB001617.

Kanamori, H., and C. R. Allen (1986). Earthquake repeat time and average stress drop, in *Earthquake Source Mechanics*, S. Das, J. Boatwright, and C. Scholz (Editors), American Geophysical Monograph 37, 227–235.

Kanamori, H., and D. L. Anderson (1975). Theoretical basis of some empirical relations in seismology, *Bull. Seism. Soc. Am.* **65,** 1073–1095.

Kanamori, H., and T. H. Heaton (2000). Microscopic and macroscopic physics of earthquakes, in *Geocomplexity and the Physics of Earthquakes*, J. Rundle, D. L. Turcotte, and W. Klein (Editors), American Geophysical Monograph 120, 147–155.

Kikuchi, M., and Y. Yamanaka (2001). Western India earthquake, http://wwweic.u-tokyo.ac.jp/index-e.html (last accessed September 2003).

Ligorria, C. P., and C. Ammon (1999). Iterative deconvolution and receiver-function estimation, *Bull. Seism. Soc. Am.* **89,** 1395–1400.

Lin, A., B. Fu, J. Guo, Q. Zeng, G. Dang, W. He, and Y. Zhao (2002). Coseismic strike-slip and rupture length produced by the 2001 M_s 8.1 central Kunkun earthquake, *Science* **296,** 2015–2017.

Mori, J. (2001). Slip distribution of mainshock, in A comprehensive survey of the 26 January 2001 earthquake (M_w 7.7) in the state of Gujrat, India, T. Sato (Editor), Report by the research team supported by the grant-in-aid for specially promoted research provided by MEXT of Japan in the fiscal year of 2000, 41–45.

Negishi, H., J. Mori, T. Sato, R. Singh, S. Kumar, and N. Hirata (2002). Size and orientation of the fault plane for the 2001 Gujrat, India, earthquake (M_w 7.7) from aftershock observations: a high stress drop event, *Geophys. Res. Lett.* **29,** 1949, doi 10.1029/2002GL015280.

Pérez-Campos, X. (2002). A comprehensive study of the seismic energy, *Ph.D. Thesis*, Stanford University, Palo Alto, California.

Pérez-Campos, X., and G. C. Beroza (2001). Mechanism dependent scaling of radiated seismic energy, *J. Geophys. Res.* **106,** 11,127–11,136.

Pérez-Campos, X., S. K. Singh, and G. C. Beroza (2003). Reconciling teleseismic and regional estimates of seismic energy, *Bull. Seism. Soc. Am.* **93,** 2123–2130.

Prejean, S. G., and W. L. Ellsworth (2001). Observations of earthquake source parameters and attenuation at 2 km depth in the Long Valley Caldera, Eastern California, *Bull. Seism. Soc. Am.* **91,** 165–177.

Rajendran, C. P., and K. Rajendran (2001). Characteristics of deformation and past seismicity associated with the 1819 Kutch earthquake, northwestern India, *Bull. Seism. Soc. Am.* **91,** 407–426.

Sato, T., and T. Hirasawa (1973). Body wave spectra from propagating shear cracks, *J. Phys. Earth* **21,** 415–431.

Savage, J. C., and M. D. Wood (1971). The relation between apparent stress and stress drop, *Bull. Seism. Soc. Am.* **61,** 1381–1388.

Singh, S. K., and M. Ordaz (1994). Seismic energy release in Mexican subduction zone earthquakes, *Bull. Seism. Soc. Am.* **84,** 1533–1550.

Singh, S. K., M. Ordaz, R. S. Dattatrayam, and H. K. Gupta (1999). A spectral analysis of the May 21, 1997, Jabalpur, India earthquake (M_w = 5.8) and estimation of ground motion from future earthquakes in the Indian shield region, *Bull. Seism. Soc. Am.* **89,** 1620–1630.

Singh, S. K., B. K. Bansal, S. N. Bhattacharya, J. F. Pacheco, R. S. Dattatrayam, M. Ordaz, G. Suresh, Kamal, and S. E. Hough (2003). Estimation of ground motion for Bhuj (26 January; M_w 7.6) and future earthquakes in India, *Bull. Seism. Soc. Am.* **93,** 353–370.

Vassiliou, M. S., and H. Kanamori (1982). The energy release in earthquakes, *Bull. Seism. Soc. Am.* **72,** 371–387.

Venkataraman, A. (2002). Investigating the mechanics of earthquakes using macroscopic seismic parameters, *Ph.D. Thesis*, California Institute of Technology, Pasadena. California, 167 pp.

Venkataraman, A., L. Rivera, and H. Kanamori (2002). Radiated energy from the 16 October 1999 Hector Mine earthquake: regional and teleseismic estimates, *Bull. Seism. Soc. Am.* **92,** 1256–1265.

Wyss, M. (1970). Apparent stress of earthquakes on ridges compared to apparent stresses of earthquakes in trenches, *Geophys. J. R. Astr. Soc.* **19,** 479–484.

Yagi, Y., and M. Kikuchi (2001). Western India earthquake, http://wwweic.u-tokyo.ac.jp/index-e.html (last accessed September 2003).

Instituto de Geofísica UNAM
Ciudad Universitaria
04510 México, DF, México
krishna@ollin.igeofcu.unam.mx
(S.K.S., J.F.P.)

Department of Science and Technology
Government of India
New Mehrauli Road
New Delhi, 110016, India
(B.K.B.)

Seismological Laboratory
California Institute of Technology
Pasadena, California 91125
(X.P.-C.)

India Meteorological Department
Lodhi Road
New Delhi 110003, India
(R.S.D., G.S.)

Manuscript received 10 October 2003.